Ultrasonics xxx (2015) xxx–xxx

Contents lists available at ScienceDirect

Ultrasonics

journal homepage: www.elsevier.com/locate/ultras

Increased range of ultrasonic guided wave testing of overhead transmission line cables using dispersion compensation

Mathew Legg *, Mehmet K. Yücel, Vassilios Kappatos, Cem Selcuk, Tat-Hean Gan

Brunel Innovation Centre, Brunel University, Uxbridge, Middlesex UB8 3PH, United Kingdom[1]

ARTICLE INFO

Article history:
Received 12 December 2014
Received in revised form 22 February 2015
Accepted 20 April 2015
Available online xxxx

Keywords:
Ultrasonic guided waves
Dispersion compensation
ACSR cables
Overhead transmission line cables
Long range ultrasonic testing

ABSTRACT

Overhead Transmission Line (OVTL) cables can experience structural defects and are, therefore, inspected using Non-Destructive Testing (NDT) techniques. Ultrasonic Guided Waves (UGW) is one NDT technique that has been investigated for inspection of these cables. For practical use, it is desirable to be able to inspect as long a section of cable as possible from a single location. This paper investigates increasing the UGW inspection range on Aluminium Conductor Steel Reinforced (ACSR) cables by compensating for dispersion using dispersion curve data. For ACSR cables, it was considered to be difficult to obtain accurate dispersion curves using modelling due to the complex geometry and unknown coupling between wire strands. Group velocity dispersion curves were, therefore, measured experimentally on an untensioned, 26.5 m long cable and a method of calculating theoretical dispersion curves was obtained. Attenuation and dispersion compensation were then performed for a broadband Maximum Length Sequence (MLS) excitation signal. An increase in the Signal to Noise Ratio (SNR) of about 4–8 dB compared to that of the dispersed signal was obtained. However, the main benefit was the increased ability to resolve the individual echoes from the end of the cable and an introduced defect in the form of a cut, which was 7 to at least 13 dB greater than that of the dispersed signal. Five echoes were able to be clearly detected using MLS excitation signal, indicating the potential for an inspection range of up to 130 m in each direction. To the best of the authors knowledge, this is the longest inspection range for ACSR cables reported in the literature, where typically cables, which were only one or two meter long, have been investigated previously. Narrow band tone burst and Hann windowed tone burst excitation signal also showed increased SNR and ability to resolve closely spaced echoes.

1. Introduction

Multi-wire cables are used in a wide range of engineering applications to meet various demands; such as load carrying in bridges and cranes, post-tensioning in concrete structures, and electric transfer in power networks. Different types of OVTL cables are used in power networks to transfer electricity over long distances. One of the most commonly used cables for high voltage overhead transmission lines are ACSR cables. To maximise heat loss, these cables generally do not have any coating covering them, but have their outer wires exposed to the elements.

Throughout their service lifetime, OVTL cables are exposed to various operational stresses (voltage and tensile) and environmental factors (wind-induced vibrations, icing, and lightning strikes). Those factors might eventually lead to structural failures such as broken insulators, corrosion, and mechanical defects (twisted/broken wires) [5,21]. Structural failures are reported to start emerging in the aluminium layers first [2]. In some cases, the steel core is reported to be intact even though aluminium layers had structural failures [5]. A reliable and preferably automated technique for the structural integrity analysis of OVTL cables is, therefore, required.

Several NDT techniques have emerged to preemptively detect the above mentioned structural integrity problems. Airborne and on-ground visual inspection is one of the most widely used techniques. However, its hazardous nature, which has led to loss of lives [15], has raised the necessity of more reliable and automated techniques. Automated visual inspection systems have been developed, which apply image processing algorithms on videos/images acquired by either aerial vehicles or stationary camera systems. However, it is reported that the efficiency of those methods relies on the quality of the camera and the stability of the aerial vehicle, which could introduce additional costs [16]. Several other systems using temperature based inspection [22], eddy current inspection [26], and radio/audible noise monitoring [8] have also been

[1] bic@brunel.ac.uk.
* Corresponding author.
E-mail address: legg.mathew@gmail.com (M. Legg).

http://dx.doi.org/10.1016/j.ultras.2015.04.009
0041-624X/

reported. More recent systems have utilised the developments in robotics [16], though design complexity, maintenance requirements and high costs have also been reported as drawbacks of such systems. In order to tackle the above mentioned drawbacks, UGW based NDT methods have been considered.

UGW, as a means of structural integrity analysis for ACSR cables, have been studied in the last few decades. Gaul et al. reported an overall feasibility analysis of the use of UGW for damage detection in ACSR cables with an emphasis on reflection of wave packets at structural discontinuities with different geometry and size [10]. Branham et al. presented an understanding of attenuation and dispersion in ACSR cables and also analysed the feasibility of defect detection in ACSR cables with two different transducer coupling schemes [4]. Haag et al. investigated UGW propagation in ACSR cables with the aim of understanding energy transfer between wires, and formulated an efficient energy-based model to predict wave propagation in a two-rod system with friction contact [12]. Baltazar et al. investigated the changes in UGW propagation in ACSR cables in the presence of a defect, and reported that the energy transfer between longitudinal and flexural wave modes can be monitored for defect detection [3].

The above mentioned studies have focused on the understanding of UGW propagation in short ACSR cables. However, for practical implementation, it is desirable to be able to inspect as long a section of cable as possible from a single location. A factor that limits the practical inspection range is dispersion. Dispersion is a phenomena where different frequency components in a signal propagate at different speeds. This causes a signal to spread out in time as it propagates. It is undesirable for UGW inspection since it reduces the SNR, reduces the ability to accurately locate defects, and can mask a defect that is close to another structure [24,25,27]. The torsional wave mode is often used since it is non-dispersive. However, this often is not a viable option and exciting only one wave mode can be difficult. Dispersion curves are, therefore, used to choose an excitation frequency range where the desired wave mode has low dispersion. Also, narrow band excitation signal, such as Hann windowed, tone bursts, are generally used. However, these signal will always have a certain bandwidth, which can lead to dispersion.

Techniques have been developed to compress received wave packets by correcting for the dispersive effects of propagation. Sicard et al. and Wilcox presented a method to compensate for the effect of dispersion from UGW signal in [20,24]. Yamasaki et al. compared experimental and simulated time-reversed square pulses for dispersion compensation [28]. Hall and Michaels performed adaptive dispersion compensation to improve imaging of defects on an aluminium plate using a distributed transducer array [13]. De Marchi et al. used a warped frequency transform to provide dispersion compensation for an irregular waveguide [7]. Zeng and Lin proposed a chirp-based dispersion pre-compe nsation technique using a priori knowledge of the propagation distance [30]. Xu et al. proposed a wideband dispersion reversal technique to self-compensate fundamental wave modes in a plate [27].

Dispersion compensation has been proposed here as a way of increasing the UGW inspection range for ACSR cables. In order to use dispersion compensation, one needs to know the dispersion curves for the medium. These are usually obtained, for structures such as pipes and plates, using commercial software such as Disperse® [14] or COMSOL® [6]. However, no software existed for generating dispersion curves for ACSR cables and it was considered to be difficult to achieve accurate results using modelling due to the complex geometry and unknown coupling between wire strands.

The approach taken was, therefore, to characterise the wave propagation using broadband Maximum Length Sequence (MLS) excitation signal and spectrograms. It was found that the signal propagated over long distances on individual outer wires of the cable as a single wave mode. These results were used to obtain a method of generating theoretical dispersion curves for the cable by correcting dispersion curves that were obtained using Disperse®. The resulting dispersion curves were used to compensate three different experimental signal, which had different bandwidths. An increased SNR and ability to resolve echoes from closely spaced structures was able to be achieved for each of these signals. The benefit of using this technique increased with inspection range. The results indicate that an inspection range of up to 130 m can be achieved using this techniques.

In Section 2, the wave propagation model and a description of the dispersion and attenuation compensation technique used in this work are presented. The experimental set up and procedure are outlined in Section 3. In Section 4, the wave propagation in the cable is investigated and theoretical dispersion curves obtained and compared to experimental results. These are used in Section 5 to dispersion compensate the measured signal to attempt to increase the inspection range for the cable.

2. Theory

In order to increase the UGW inspection range on the ACSR cable, it was considered important to understand the ultrasonic wave propagation in the cable. By understanding the propagation characteristics, which lead to a reduction in the inspection range, signal processing algorithms can be implemented to attempt to compensate for these effects. In Section 2.1, a basic wave propagation model is presented, which was thought to provide an approximate model of the wave propagation in the cable. A dispersion compensation algorithm, based on equations given in Refs. [20,24], is then outlined in Section 2.2.

2.1. Wave propagation model

Consider a signal $h(t)$ excited by a transducer, which causes a single wave mode to be excited. After propagating a distance d, the resulting signal $g(t)$ may be approximated in the frequency domain by

$$G(\omega) = H(\omega)\exp\left(-[\alpha + jk(\omega)]d\right) + E(\omega), \tag{1}$$

where ω is the angular frequency, $H(\omega)$ is the Fourier transform of $h(t)$, α is the propagation attenuation coefficient, k is the wave number, and $E(\omega)$ is noise. The wave number may be calculated using

$$k = \frac{\omega}{v_{ph}}, \tag{2}$$

where v_{ph} is the phase velocity. If multiple wave modes are excited, then the signal will be the sum of all these wave modes, each of which may be approximated by Eq. (5), where H, α, and k are different for each wave mode.

The velocity that the wave packet propagates at is the group velocity. For a narrow band signal, the time axis t of the signal may be converted to distances d using

$$d(t) = v_{gr}(\omega_p)t, \tag{3}$$

where $v_{gr}(\omega_p)$ is the group velocity at a single angular frequency ω_p corresponding to the highest amplitude component of $G(\omega)$. For a dispersive wave mode, the phase and group velocity are frequency dependant. This means that different frequency components in the signal propagate at different speeds causing the signal to spread out in time as it propagates. This reduces the SNR, which limits the inspection range and reduces the spatial resolution. Dispersion compensation can be used to correct for this effect.

Please cite this article in press as: M. Legg et al., Increased range of ultrasonic guided wave testing of overhead transmission line cables using dispersion compensation, Ultrasonics (2015), http://dx.doi.org/10.1016/j.ultras.2015.04.009

2.2. Signal processing to compensate for effects of propagation

Consider that an attenuated, dispersed signal $\hat{g}(t)$ is sampled. Compensation for the effects of attenuation may be made using

$$g(t) = \hat{g}(t)\,\exp(\alpha t), \tag{4}$$

[31]. For a single wave mode and the i_{th} propagation time (or distance), dispersion compensation can be performed in the frequency domain using

$$Y(\omega, t_i) = G(\omega)\exp\left(j[k(\omega)d(t_i) - \omega t_i]\right), \tag{5}$$

where d is the propagation distance. Eq. (5) is calculated for each frequency component in the signal. An inverse Fourier transform

$$\hat{y}(t) = \text{IFFT}\{Y_m(\omega, t_i)\}, \tag{6}$$

is then used to convert the dispersion compensated signal to the time domain. Note that without the term "ωt_i" in Eq. (5), the signal originally at time t_i would be shifted back to the origin in the time axis for the dispersion compensated signal. This technique will theoretically provide the correct amount of dispersion compensation of the signal $g(t)$ at time t_i but will under or over correct for other times.

In this work, to correct all of the signal, Eqs. (5) and (6) were run in a loop over all times, where the i_{th} iteration performed dispersion compensation for the i_{th} time in the signal $\hat{y}(t_i)$. This value was taken and used to create the i_{th} value of a new array $y(t_i)$. This enabled a dispersion compensated version of $g(t)$ to be created for all times. This method is relatively slow. Faster methods, such as that described in [24], could be used instead.

2.3. Excitation signals

The amount of dispersion that a dispersive UGW wave mode experiences during propagation along a structure is related to the bandwidth of the signal. The wider the bandwidth of the signal, the more dispersion will occur. Therefore, to test the benefit of using dispersion compensation for improving the inspection range, three different types of signal have been used, which had different frequency bandwidths. In order of decreasing bandwidth, these signals were Maximum Length Sequences (MLS) white noise, tone burst, and Hann windowed tone burst.

Maximum length sequences are composed of either +1 or −1 values. They are generated using Linear Feedback Shift Registers (LFSR) with N-delay taps, resulting in a sequence of length $L = 2^N - 1$ [11]. They are wideband with a flat spectral density from DC to half the analogue sampling frequency used to generate the signal. These frequency components are evenly distributed through the signal giving it a time invariant frequency response. This makes MLS more convenient for imaging the dispersion in a signal using spectrograms than signals, such as a chirp, which have a frequency response that varies with time. Also, they have a δ-function like autocorrelation function meaning that the use of cross-correlation to improve spatial location of defects is a potential option. More information about m-sequences can be found in Ref. [19]. The MLS signal used for this work was generated using code by Wiens [23].

A tone burst consists of a number of cycles of a sine wave. In order to increase the spatial resolution, only a few cycles are generally used. However, the fewer the number of cycles, the wider the bandwidth of the signal will be. To reduce this bandwidth, Hann windowing of the tone burst signal is generally applied. These narrow bandwidth signals are the most commonly used excitation signal for UGW inspection of structures, since their narrow bandwidth minimises the amount of dispersion that occurs. Tone burst and Hann windowed tone burst excitation signals have, therefore, been utilised in this work to provide signals with two different bandwidths compared to MLS and also to see if dispersion compensation can provide increased inspection range with these narrow bandwidth signals.

3. Experimental setup

3.1. Cable

3.1.1. Cable characteristics

The cable used in this study was a 26.5 m long, Bear 325 ACSR cable. In order to simulate a defect in the cable, a cut was introduced into the cable 1.5 m from the end of the cable, see Fig. 1. The cut depth was 6 mm deep at the time that the measurements were made for this work. However, cut depths as small as 2.5 mm had been previously investigated and were able to be detected using UGWs.

The Bear 325 cable is composed of steel and aluminium wire strands, which are 3.4 mm in diameter. At the centre of the cable are seven steel wires, which are coated in grease. Over this are two layers of aluminium wires, which respectively have 12 and 18 strands in each layer. The outer diameter of each layer of wires in the cable are respectively 10.05, 16.65, and 23.24 mm.

The wires are twisted around the cable into a helical shape, with each layer being twisted in the opposite direction. This means that the length of a wire L_w is longer than the length of the cable L_c by the ratio

$$\frac{L_w}{L_c} = \frac{\sqrt{(\pi D)^2 + p^2}}{p}, \tag{7}$$

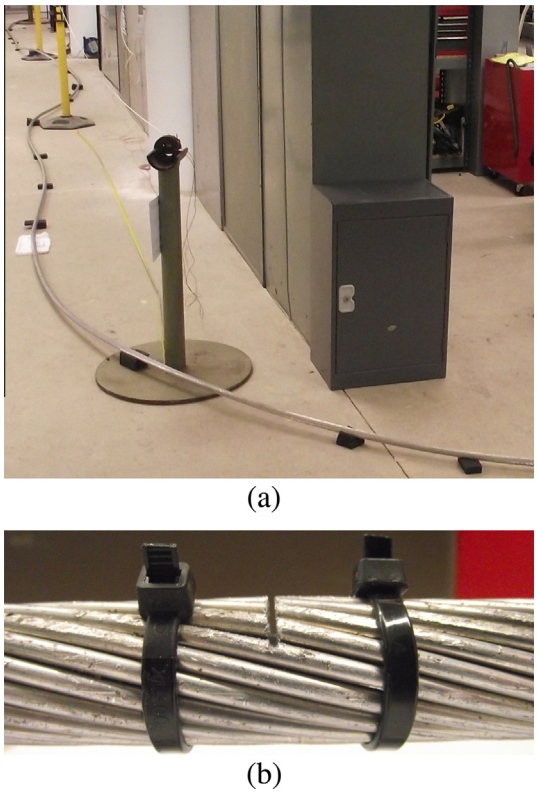

(a)

(b)

Fig. 1. Photo (a) shows the 26.5 m long Bear ACSR cable used in this study. It was laid out on the floor of the lab with foam pads keeping it off the ground. Photo (b) shows a 6 mm deep cut made into the cable 1.5 m from one end of the cable to simulate a defect.

Please cite this article in press as: M. Legg et al., Increased range of ultrasonic guided wave testing of overhead transmission line cables using dispersion compensation, Ultrasonics (2015), http://dx.doi.org/10.1016/j.ultras.2015.04.009

where D is the diameter of the layer in which the wire is located and p is the pitch or distance along the cable required for the wire to make a full rotation around the cable. The pitch of the outer aluminium wire layer was 300 mm.

3.2. Hardware

3.2.1. Transducer collar

Shear transducers made by Plant Integrity [18] were used in this work. They consisted of a PZT ceramic element mounted into a stainless steel backing, see Fig. 2(a). The natural frequency of the PZT element is in the MHz range. However, the use of the backing mass makes the transducer broadband. They are reported to have a relatively flat gain in the frequency range of interest (20–500 kHz). Refer to Ref. [9] for more information on these transducers.

Six of the shear transducers were mounted in a collar so that they were evenly distributed around the circumference of the cable, see Fig. 2. No coupling agent was used. Instead the transducers are pushed against the cable using springs. This is referred to as dry coupling. Adjacent pairs of transducers were wired in parallel. This gives three channels used for both transmission (TX) and reception (RX).

3.2.2. Ultrasound pulser/receiver unit

The transducer channels were connected to three channels of a Teletest® [17,18], a commercial Long Range Ultrasonic Testing (LRUT) system. This unit was connected to a laptop and controlled using data acquisition software. The transducer array was driven with a user defined waveform with an analogue output sampling rate of 1 MHz and an amplitude of 280 V_{pp}. The resulting signal measured by the transducers was amplified by a factor of 37 dB and filtered using an analogue bandpass filter with corner frequencies of about 1 and 600 kHz. The filtered signal was then sampled with an analogue input sampling rate of 1 MHz. This was repeated a number of times and the resulting signal averaged and saved to file.

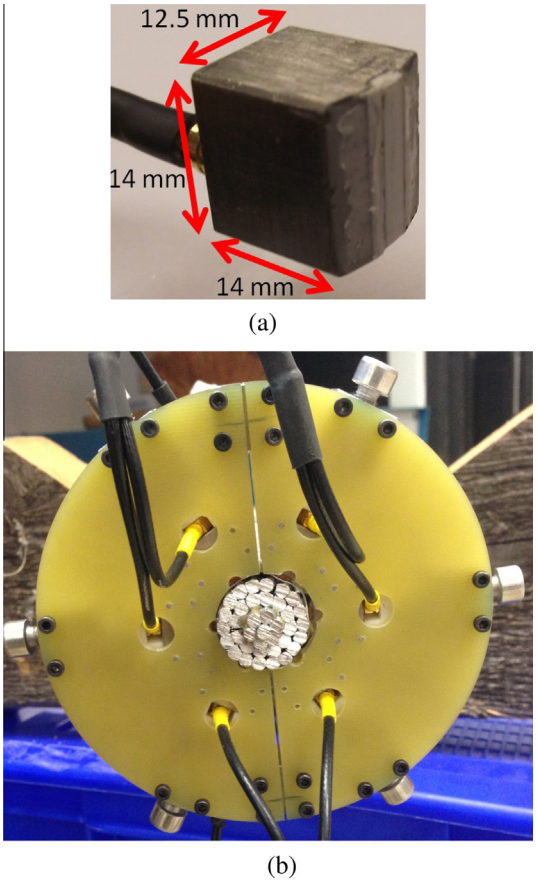

Fig. 2. Photos of a shear transducer (a) and the transducer collar used to generate and receive UGW signals on the cable.

3.3. Measurement procedure

The transducer collar was initially positioned at the end of the cable, at the opposite end from the cut, and used in a pulse echo configuration. Three types of excitation signal were used; MLS, tone burst, and Hann windowed tone burst. The MLS was generated in Matlab and the first 50 samples of the resulting sequence were used. Since the transmit sampling rate was 1 MHz, this signal had a transmit period of 50 μs and had a flat frequency response from 0 to 500 kHz. The tone burst and Hann windowed tone burst excitation signals consisted of five cycles of a sine wave with a central frequency of 240 kHz. All three excitation signals were applied to the transducers with an amplitude of 280 V_{pp}. The resulting signal measured on the three transducer channels were recorded and saved to file.

4. Investigating wave propagation in the cable using MLS signal

The recorded signals were processed using Matlab. The three transducer channels were summed to give a single time domain signal. Fig. 3(a) shows an example time domain signal measured on the cable using MLS excitation. The first echoes at approximately 10 ms appear to be reflections from the cut and the end of the cable. The first echo has an amplitude of approximately 2.5 time that of the second echo. This might be explained by the fact that a significant amount of the signal is reflected from the cut. This would reduce the energy reaching the end of the cable, potentially causing a smaller amplitude echo from the end of the cable compared to that from the cut. There may also be some reduction in amplitude of the second echo due to destructive interference of the cut and end echoes. A second set of echoes can only

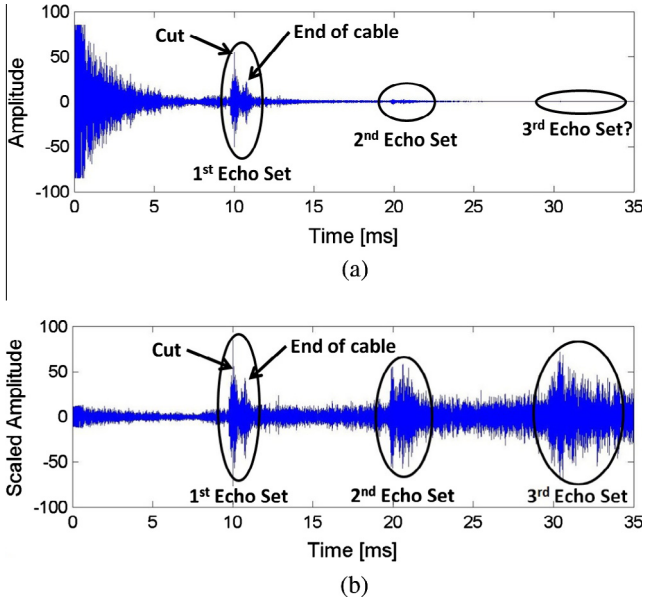

Fig. 3. Plot (a) shows an example time domain signal obtained using MLS signal. An exponentially scaled version of this plot is shown in plot (b). Peaks in the signal, which are assumed to be the first echo from the cut and the end of the cable, are indicated on the plots.

Please cite this article in press as: M. Legg et al., Increased range of ultrasonic guided wave testing of overhead transmission line cables using dispersion compensation, Ultrasonics (2015), http://dx.doi.org/10.1016/j.ultras.2015.04.009

just be seen at approximately 20 ms, while it is not clear if there is a third echo set. In order to increase the range of inspection, the signal $g(t)$ was scaled with time t using Eq. (4). The resulting scaled signal is plotted in Fig. 3(b). As a result of the scaling, three sets of dispersed echoes can now be seen, though they are increasingly blurred with time or propagation distance along the cable.

The attenuation coefficient α that was used to obtain the scaled signals shown in Fig. 3(b) was 265. This was chosen using trial and error to give the echoes in the scaled signal similar amplitudes. This trial and error method assumes that the losses due to reflections and any potential mode conversions are small compared to the attenuation losses during propagation along the cable. This assumption appeared to be sufficient for increasing the ability to detect defects. However, if a more accurate attenuation coefficient was desired, these losses should be measured and included in the propagation model.

4.1. Time–frequency analysis

A time–frequency representation of the signal can be obtained using spectrograms. Spectrograms are a time–frequency plot obtained using using Short-Time Fourier Transforms (STFT). Fig. 4 shows a spectrogram of the exponentially scaled signal obtained using MLS excitation. The time length that was used in the STFT to generate this figure was 512 μs. The echoes from the cut and the end of the cable can be seen as sets of curved lines (peaks) in the spectrogram at about 10, 20, and 30 ms. Since these curves have roughly the same shape, it appears that these are due to a single wave mode. The fact that these curves are increasingly deflected from the vertical with propagation distance means that this wave mode is experiencing dispersion. However, without modelling, it is unclear if the wave mode is a longitudinal, flexural, or torsional wave mode or indeed if there is really only one wave mode present in the signal.

4.1.1. Experimental measurement of dispersion curves

Dispersion causes the SNR of the signal to reduce with propagation distance along the cable and represents a significant limitation to the inspection range that can be achieved using UGW inspection. Dispersion compensation is proposed as a means of increasing the inspection range achievable from a single location. In order to perform dispersion compensation, one needs to know the dispersion curves for the cable. For structures with simple cross-sectional geometries, such as plates, rods, and pipes, these would traditionally be obtained analytically using software such as Disperse®. Alternatively, for structures with more complex geometries, Finite Element Analysis (FEA) modelling software, such as COMSOL®, are sometimes used with eigenfrequency analysis to find phase velocity dispersion curves. However, these are not always accurate. For the ACSR cables, the complex coupling between multiple wire stands in the cable meant that accurately modelling the cable as a whole was very difficult. This meant that the dispersion curves needed to be measured experimentally.

A group velocity dispersion curve for the cable was measured by fitting peaks in the spectrogram data corresponding to echoes from the cut in the cable. To reduce the echo from the end of the cable, time domain data was measured on one of the three transducer channels that had a comparatively higher echo from the cut than that from the end of the cable. A spectrogram was obtained of this data for the time period around the first echo. Peaks in the spectrogram data were then obtained in the frequency range where strong echo frequency components were present between approximately 115 and 450 kHz. A k_{th} nearest neighbour search was used to identify isolated peaks. These were regarded as noise and were removed. Fig. 5 shows the spectrogram with the denoised points and a fitted curve overlaid. This gives measurements of the arrival times $\tau(\omega)$ of the signal from the cut. Measured group velocities were then obtained by

$$v_{gr}(\omega) = \tau(\omega)/L, \tag{8}$$

where L was the propagation distance along the length of the cable, which was twice the distance from the transducer array to the cut.

4.1.2. Correspondence between measured and analytical dispersion curves

Spectrograms, with MLS excitation signal, provide a useful method of investigating wave propagation characteristics. However, without modelling, it can be difficult to explain what wave modes are present. Also, the measured dispersion curves obtained using this method would be expected to be different for different types of cables. It is, therefore, desirable to have an analytical way of obtaining the dispersion curves.

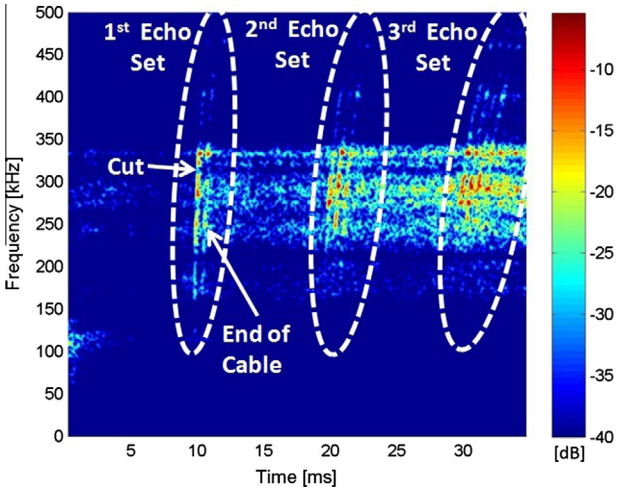

Fig. 4. Spectrogram of the scaled time domain signal shown in Fig. 3(b). The echoes can be seen as near virticle lines which curve slightly to the right with increased frequency. This curvature shows the dispersion in the signal. Three sets of echoes can be seen in the data. The first set are the first echoes from the cut and the end of the cable.

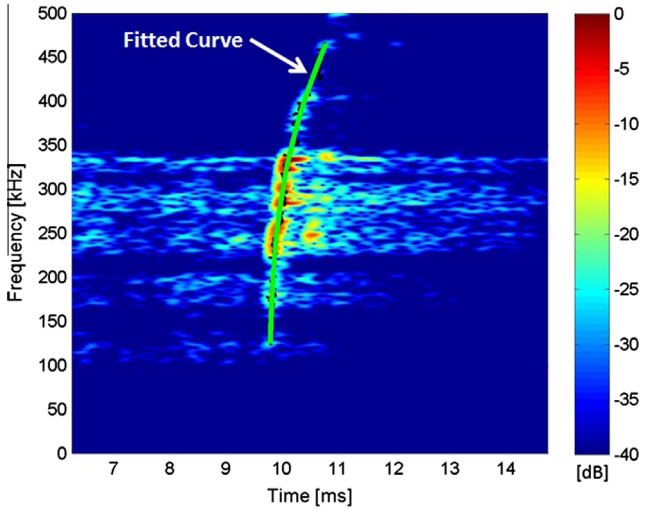

Fig. 5. Spectrogram of a section of time domain signal measured on one of the three transducer channels using MLS excitation. The black dots show peaks obtained from this data for the first echo from the cut near the end of the cable. Overlaid on this is a fitted dispersion curve (green line). (For interpretation of the references to colour in this figure legend, the reader is referred to the web version of this article.)

Please cite this article in press as: M. Legg et al., Increased range of ultrasonic guided wave testing of overhead transmission line cables using dispersion compensation, Ultrasonics (2015), http://dx.doi.org/10.1016/j.ultras.2015.04.009

Laser scanning vibrometer experiments had been performed to image the wave propagation on the surface of the cable. This had shown that the ultrasonic waves tend to propagate mainly along individual wires, see Fig. 6(a). Therefore, experimentally measured dispersion curves for a single wire were obtained. This was performed by making a vibrometer scan at evenly spaced points along the surface of the wire for a MLS excitation signal. The resulting time domain data were formed into a matrix, where the n_{th} row was the signal measured at the n_{th} scan point. A 2D FFT was the applied and the resulting wave number – frequency domain matrix was plotted, see Fig. 6(b). Refer to Ref. [1] for more details on this technique. Software called Disperse® was used to generate theoretical dispersion curves for aluminium rods that were the same diameter as the wires in the cables. These were overlaid over the experimentally measured dispersion curves. The results showed that the longitudinal mode was the dominant wave mode, with the flexural mode able to be clearly seen in the data. Although not shown in this plot, the torsional wave mode could also be faintly observed in some of the scan data. The theoretical group velocity dispersion curves provided a good fit to the data for all three wave modes.

These dispersion curves needed to be corrected for the effect of the helical twist of the wires making up the cable. The length of the cable was shorter than the length of the wires. This means that the apparent velocity along the cable would be slower than the velocity in individual wires. To correct for this, the theoretical dispersion curves were scaled by dividing them by the length ratio given in Eq. (7). The theoretical group velocities for the cable were, therefore, calculated using

$$v_{gr} = \frac{v_{gr}^{\dagger}\, p}{\sqrt{(\pi D)^2 + p^2}}, \tag{9}$$

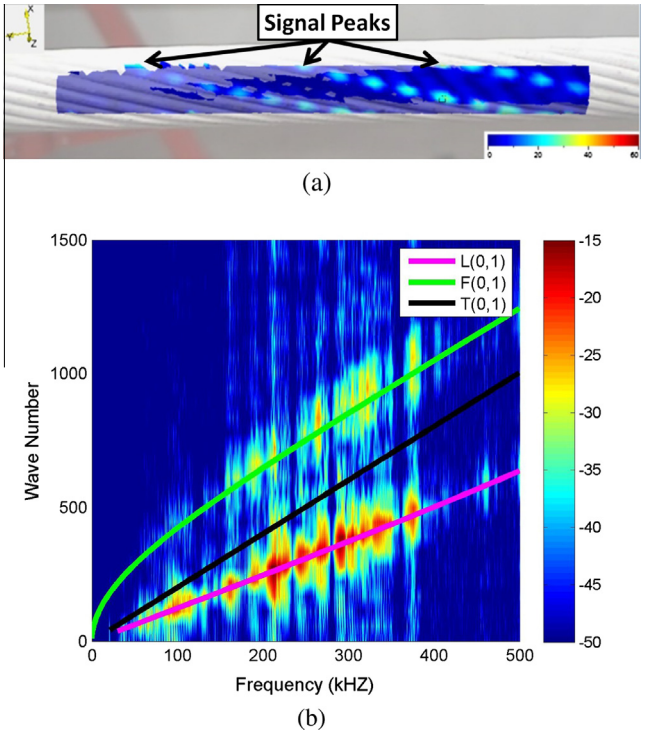

Fig. 6. Image (a) shows a laser scanning vibrometer scan of the surface of a 2 m long cable when transmitting a 250 kHz Hann windowed tone burst excitation signal. It can be seen that the ultrasonic waves appear to propagate along individual wires of the cable. Plot (b) shows experimentally measured dispersion curves obtained using a laser vibrometer scan of a single wire for a MLS excitation signal. Overlaid are the theoretical dispersion curves for a single aluminium wire.

where $v_{gr}^{\dagger}$ is the theoretical group velocity of the rod obtained using Disperse®, D is the diameter of the wire layer, and p is the pitch of the cable.

Fig. 7 shows the measured group velocity data points obtained from the spectrogram in Fig. 5. Overlaid on this are the theoretical group velocity dispersion curves corresponding to the $L(0,1)$ wave mode for aluminium rods which has been corrected for three different helical twist diameters; inner and outer aluminium wire layer diameters, and the mean of these two. It can be seen that the experimental data lie mainly between the lines corresponding to the inner and outer diameters. The line corresponding to the centre of the two aluminium layers provides a good fit to the measured data. This indicates that the dispersion curves for ACSR cables can be obtained analytically by calculating the dispersion curves for individual wires and then correcting these for the effect of the helical twist. Fig. 8 shows the original and helical corrected theoretical group velocity dispersion curves for the aluminium wires in the cable obtained using Disperse®.

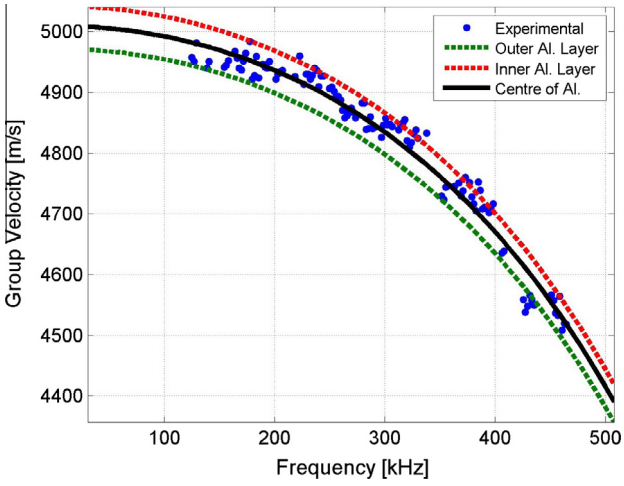

Fig. 7. Group velocity dispersion curve experimental measured data points (blue dots) from Fig. 5. Overlaid on this are the group velocity dispersion curve data for the $L(0,1)$ wave mode of aluminium rods obtained using Disperse® software which has been corrected for the helical twist for three different diameters using Eq. (9). (For interpretation of the references to colour in this figure legend, the reader is referred to the web version of this article.)

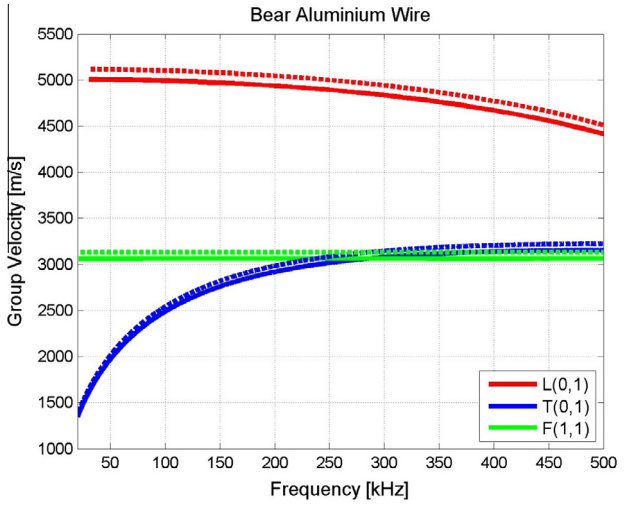

Fig. 8. Original (dashed lines) and helical corrected (solid lines) theoretical group velocity dispersion curves for aluminium wires in the cable showing longitudinal $L(0,1)$, torsional $T(0,1)$, and flexural $F(1,1)$ wave modes obtained using Disperse®.

Please cite this article in press as: M. Legg et al., Increased range of ultrasonic guided wave testing of overhead transmission line cables using dispersion compensation, Ultrasonics (2015), http://dx.doi.org/10.1016/j.ultras.2015.04.009

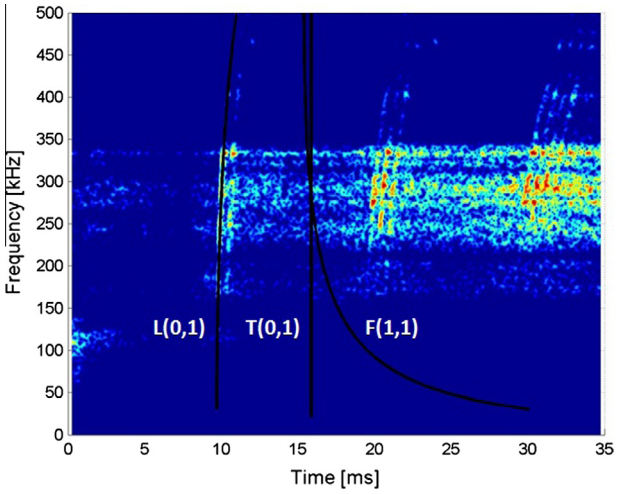

Fig. 9. Spectrogram of MLS excitation signal. Overlaid are theoretical arrival times obtained using the dispersion curves calculated in Section 4.1.2 for the longitudinal $L(0,1)$, torsional $T(0,1)$, and flexural $F(1,1)$ wave modes.

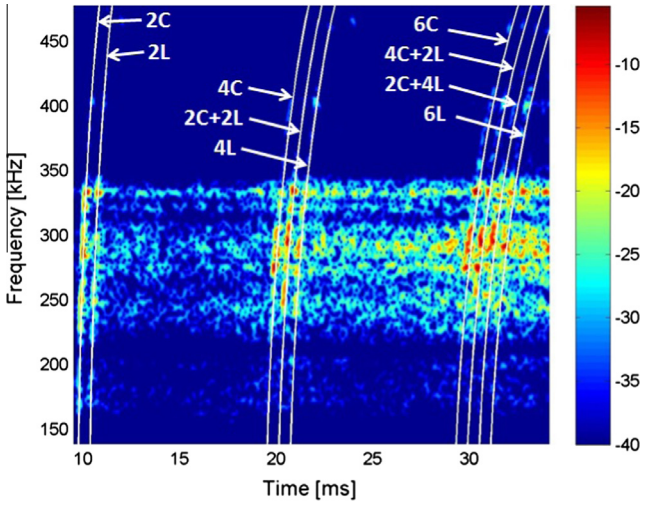

Fig. 10. Spectrogram of the signal obtained using MLS excitation. Overlaid on top are the arrival times (white lines) calculated using the propagation distances shown in Table 1 and the theoretical group velocity dispersion curve for the aluminium longitudinal wave mode.

Table 1
Table of distances used to calculate the arrival times for the three sets of echoes in Fig. 10. The distances C and L are respectively the distance from the array to the cut (25 m) and to the end of the cable (26.5 m).

Echo set no.	Line 1	Line 2	Line 3	Line 4
1	$2C$	$2L$		
2	$4C$	$2C+2L$	$4L$	
3	$6C$	$4C+2L$	$2C+4L$	$6L$

4.1.3. Identification of wave modes in the spectrograms

The theoretical dispersion curves obtained in the previous section were used to identify what wave modes were present in the signal measured on the cable. Fig. 9 shows a spectrogram of this signal. Overlaid over this are the expected arrival times, for the first echo from the cut, which were calculated using the theoretical dispersion curves for the aluminium wires. As had been found in the previous section, the longitudinal wave mode arrival times show good agreement with peaks in the spectrogram. However, the theoretical arrival times of the flexural and torsional wave modes do not appear to correspond to any significant peaks in the spectrogram. To check that summing the three receiver channels was not omitting the flexural wave mode, this process was repeated using a single channel (two adjacent transducers wired in parallel). However, again only the longitudinal wave mode was observed in the spectrogram. This is in contrast to measurements on shorter lengths of cables (about 2 m long), where the flexural wave mode was able to be seen in the spectrogram [29]. This indicates that the flexural wave mode experienced high attenuation rates compared to the longitudinal wave mode.

The result shown in Fig. 9 appears to indicate that the peaks in the spectrogram corresponded to the longitudinal wave modes. To test this, the theoretical arrival times for the first three sets of echoes from the cut and end of the cable were calculated using the theoretical longitudinal wave mode group velocities and the propagation distances given in Table 1. These were then plotted over the spectrogram, see Fig. 10. For the first echo set, there are two reflections, one from the cut and one from the end of the cable. For the second echo set, there are three echoes. This corresponds to the three possible propagation paths. The signal can be reflected twice off the cut, once off the cut and once off the end of the cable, or twice off the end of the cable. Using the same principle, one can explain why the third echo set has four echoes. It can be seen that the theoretical arrival times are in good agreement with the data.

The lack of echoes corresponding to the steel wires seems to indicate that there is poor coupling between the steel and aluminium wires in the cable. This appeared to be confirmed by a laser vibrometer scan of the end surface of the cable next to the transducer collar. This showed a significant decrease in amplitude of signal in the steel core. The reason for this is not clear. The presence of the grease surrounding the steel wires could provide poor transfer of shear motion from the aluminium to steel wires. The wires in each layer are twisted in opposite directions. This angle between layers may mean that the longitudinal motion of wires in one layer will not be optimally passed on to wires in the next layer. Also, the loose nature of the untensioned cable could mean that there is poor contact between wire layers.

The results presented in this work show that a single wave mode can propagate over large distances on individual aluminium wires of the cable. It was found that the wave propagation could be described by the longitudinal wave mode of an aluminium wire when it was correction for the helical twist of the cable. However, it is not clear if this would still be the case if the cable was in tension. Further work is needed to characterise the wave propagation when the cable is under tension. Studies should also investigate different types of ACSR cables to see if similar wave propagation behaviour is observed with these cables.

5. Dispersion compensation results

Fig. 10 shows that, with time scaling, the echoes from defects in the cable show up clearly in a spectrogram for at least the first three echoes from the end of the cable. However, due to dispersion, these signals are spread out in the time domain resulting in reduced signal to noise ratio with propagation distance, see Fig. 3(b). In theory, dispersion compensation should be able to correct for this. This section looks at the effect of dispersion compensation of signal measured on the cable for MLS, tone burst, and Hann windowed tone burst signal.

5.1. MLS white noise

The dispersion compensation algorithm described in Section 2.2 was applied to the exponentially scaled signal obtained for MLS

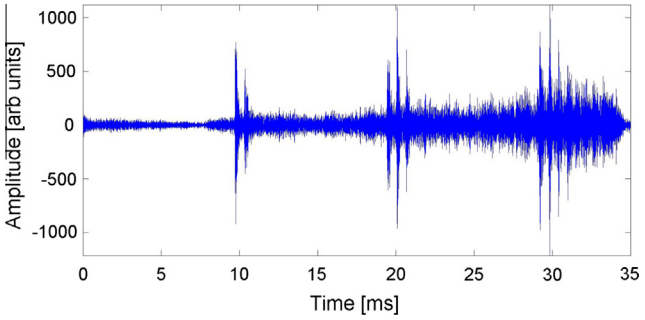

Fig. 11. Plot showing the dispersion compensated signal measured on the cable for MLS excitation signal.

excitation, see Fig. 3(b), using the theoretical dispersion curves obtained in Section 4.1.2. Fig. 11 shows the resulting dispersion compensated signal. Fig. 12 shows the Hilbert transform of the dispersed and dispersion compensated signals. An increase in SNR of between 4 and 8 dB is achieved. However, the main benefit is the fact that the individual echoes are able to be seen in the dispersion compensated signal, which cannot be distinguished in the dispersed signal. The gain in ability to resolve individual peaks is from 7 to at least 13 dB. A spectrogram of this dispersion compensated data is shown in Fig. 13. It can be seen that the effect of the dispersion compensation was to make the echo curves vertical in the spectrogram.

An A-scan like time trace can be made from the spectrogram data. The spectrogram data, which have units of dB, form a $M \times N$ matrix, where M is the number of frequencies and N is the number of times. A time trace signal in the form of a $1 \times N$ vector can be achieved by summing down the columns (frequency components) of this matrix. Fig. 14 shows the resulting time trace for both the dispersed and dispersion compensated signal. Since the dispersion echo lines are not vertical in the spectrogram data, this technique gives blurred (dispersed) A-scan peaks for these echoes and a reduction in SNR with propagation distance. In contrast, the dispersion compensated signal are vertical in the spectrogram. This results in sharp peaks occurring for each individual echo and an increased SNR. It appears that dispersion compensation has the potential to increase the inspection range possible from a single location.

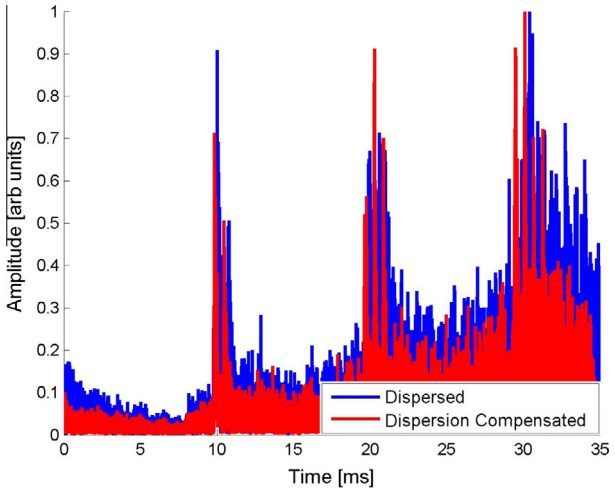

Fig. 12. Plot showing the normalised Hilbert transform of the dispersed and dispersion compensated signals measured on the cables for MLS excitation signal.

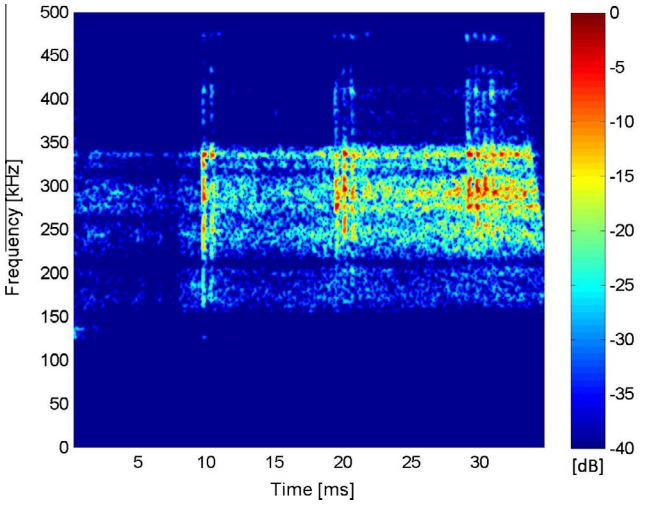

Fig. 13. Spectrogram of this dispersion compensated signal obtained using MLS excitation.

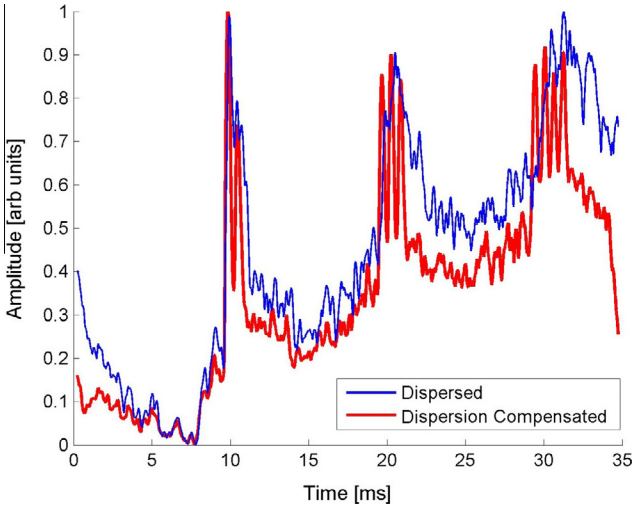

Fig. 14. Normalised time traces obtained by summing the columns of the spectrograms for the dispersed and dispersion compensated signal for a MLS excitation signal.

5.1.1. Long range MLS recording

To test the potential range that could be achieved using this technique, a longer recording of 60 ms was made for the MLS excitation signal. This was the longest recording able to be made using the data acquisition hardware. In an attempt to make the echoes less complicated for the longer recording, efforts were made to reduce the echoes from the cut. Guided waves are reflected when they encounter a change in cross sectional area in a structure. Therefore, a band of metal (pipe clamp) was attached around the cable covering the cut to compensate for the change in cross-sectional area caused by the cut and to acoustically link the wires on each side of the cut.

The noise floor had a larger effect on the exponentially scaled signal for the longer recordings. This appeared as horizontal lines in the spectrogram, which become exponentially scaled with increasing time. A possible source of these spectral lines was thought to be nearby switch mode power supplies. To reduce this, these noise spectral lines were manually identified and removed. Also, frequency components outside a frequency range of 160–400 kHz were also removed. Fig. 15 shows the exponentially scaled

Please cite this article in press as: M. Legg et al., Increased range of ultrasonic guided wave testing of overhead transmission line cables using dispersion compensation, Ultrasonics (2015), http://dx.doi.org/10.1016/j.ultras.2015.04.009

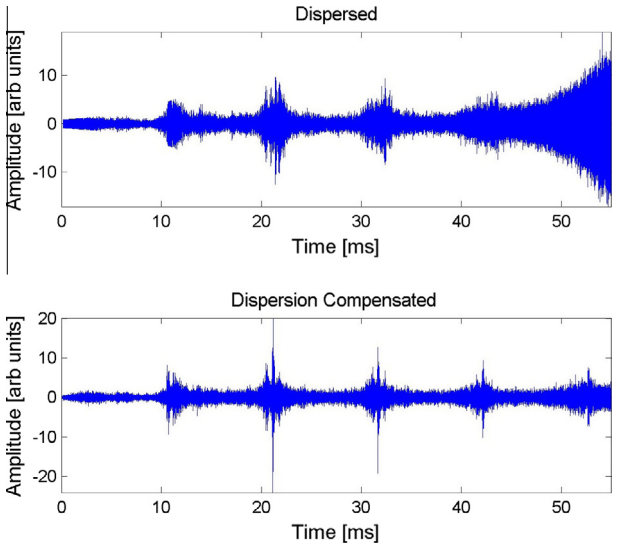

Fig. 15. Plots of the time domain dispersed and dispersion compensated filtered signal obtained for the long recording of the MLS excitation signal.

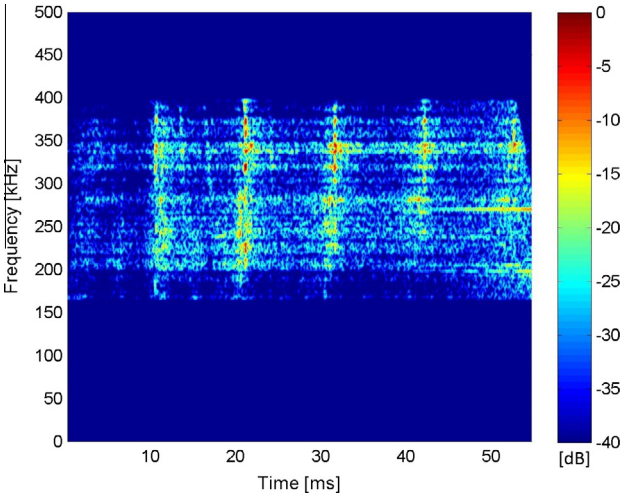

Fig. 16. Spectrogram of the dispersion compensated signal obtained for the longer recording using MLS excitation signal.

and dispersion compensated signal. The echoes are sharper and there is an increased SNR for the dispersion compensated signal.

Fig. 16 shows the spectrogram of the dispersion compensated signal. The A-scans obtained from the spectrograms of the dispersed and undispersed signal is shown in Fig. 17. The dispersion compensation had the effect of increasing the clarity of the echoes and increases the SNR compared to the dispersed signal. It can be seen that five echoes from the end of the cable can be seen with some weaker echoes from the covered cut. This theoretically corresponds to an inspection range of 130 m. This shows that the combination of exponential scaling, dispersion compensation, and filtering can effectively increase the inspection range for a broad band signal.

5.2. Narrow bandwidth signal

Dispersion compensation was performed for narrow band signal to see if a similar improvement in SNR could be achieved, as was observed for the broadband MLS signal. Recordings were made using five cycle tone burst and Hann windowed tone burst

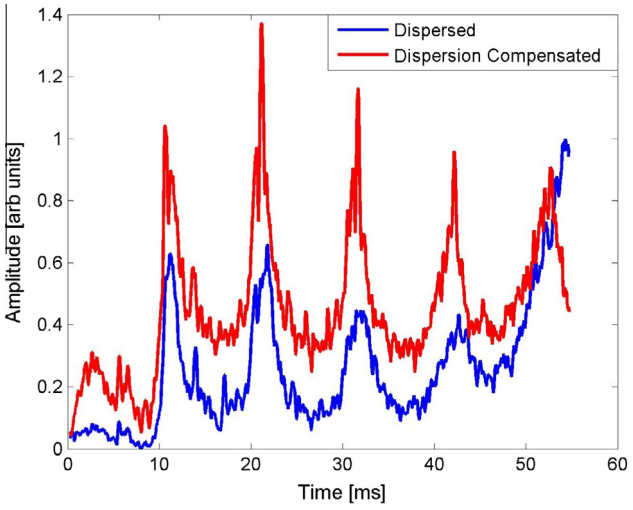

Fig. 17. A-scan time trace of the dispersed and dispersion compensated filtered signal for the longer recording of the MLS excitation signal.

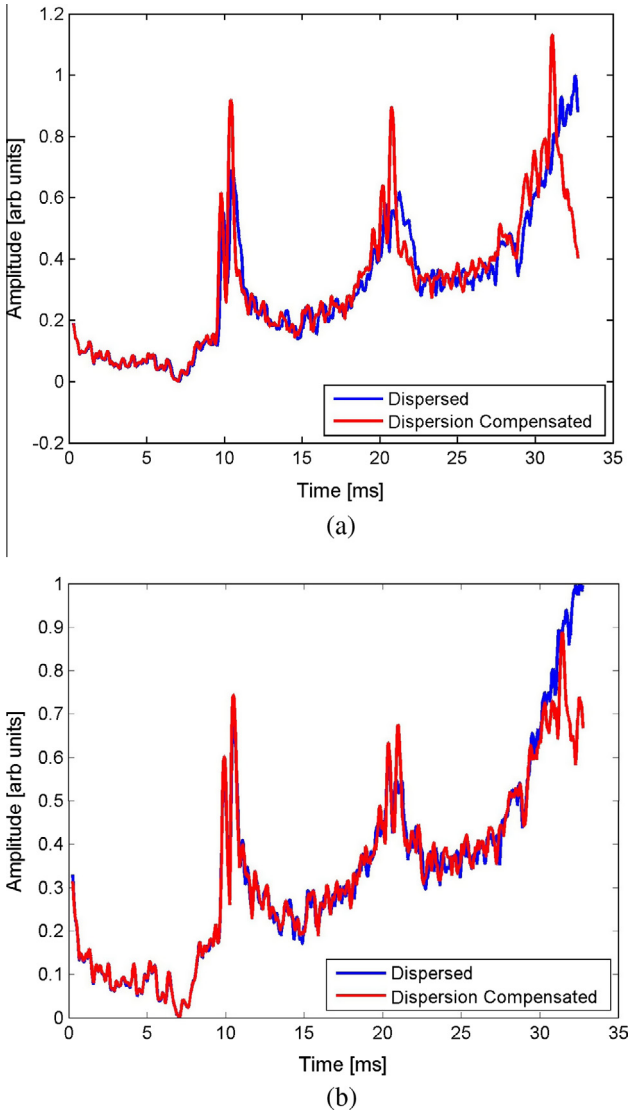

Fig. 18. A-scan of the dispersed and dispersion compensated signal obtained using (a) tone burst and (b) Hann windowed tone burst excitation signal with a central frequency of 240 kHz.

excitation signal with a central frequency of 240 kHz. The same experimental set up as in Section 5.1.1 was used for these recordings. Dispersion compensation was then performed for these two types of signal. Fig. 18 shows the dispersed and dispersion compensated A-scans for the tone burst and Hann windowed tone burst excitation signal. It can be seen that an increase in SNR was achieved for both signals.

6. Conclusion

LRUT has previously been proposed as a possible NDT technique for the inspection of ACSR cables. Studies have shown that UGWs can detect defects in ACSR cables. However, to the best of the authors' knowledge, this is the first study to investigate lengths of cables longer than about two meters long. This work investigated ultrasonic wave propagation on a 26.5 m long length of ACSR cable, which was not under tension. Measurements showed that, with correction for attenuation, several echoes could be detected from the end of the cable and a cut, which was located 1.5 m from the end. However, due to dispersion, there was a decreased SNR and decreased ability to resolve individual echoes as the propagation distance increased. Dispersion compensation was proposed as a method for correcting for these effects and thereby increasing the effective UGW inspection range for these cables.

In order to implement dispersion compensation, one needs dispersion curves for the structure being investigated. No software existed for obtaining the dispersion curves for ACSR cables and it was considered to be difficult to achieve accurate results using modelling due to the complex geometry and unknown coupling between strands. Group velocity dispersion curve data was, therefore, measured experimentally. A novel method for obtaining theoretical dispersion curves for the cable was then developed. For propagation distances more than a few meters, it was found that the fundamental longitudinal mode $L(0,1)$ for aluminium was the only wave mode observed in the signal. The theoretical dispersion curve data was then used to perform dispersion compensation. It was found that an increase in SNR of 4–8 dB was observed compared to the dispersed signal. However, the main benefit was an increased ability to resolve echoes from closely spaced structures; the end of the cable and an adjacent cut. Without dispersion compensation, only the first set of echoes could be clearly resolved. With dispersion compensation and some filtering, individual echoes could be distinguished clearly for at least five sets of echoes from the end of the cable. This would indicate an inspection range of up to 130 m in each direction might be achievable. Dispersion compensation was also applied to narrow band signal and increased SNR and ability to resolve closely spaced echoes was obtained for these signals. While this study used an ACSR cable, this technique could be used for increasing the LRUT inspection range for other structures, such as plates, pipes, and other types of cables.

More work is needed to investigate the wave propagation on different types of ACSR cables in conditions which are more representative of those that would be experienced in testing of overhead transmission lines. These cables are under tension, conduct high voltage electricity, have higher operating temperatures, and would be expected to experience larger background noise conditions. These factors, particularly tension, need to be investigated further to see what effect they have on wave propagation and the effective range, which can be achieved in these conditions.

Acknowledgements

The CHAPLIN project is funded by the European Commission under the 7th Framework Programme (FP7) Research for the benefit of specific groups – Research for SMEs Grant Agreement Number 315130. Chaplin is collaboration between the following organisations: Robotnik Automation S.L.L., Dasel Sistemas S.L, DTK Electronics Ltd., Albatroz Engenharia, TWI Ltd., Innora Robotics and Automation S.A. and Brunel University. Authors would like to acknowledge Makis Livadas of BIC and Nigel Lee of TWI for technical guidance.

References

[1] D.N. Alleyne, P. Cawley, A two-dimensional Fourier transform method for the measurement of propagating multimode signals, J. Acoust. Soc. Am. 89 (1991) 1159.
[2] C. Azevedo, T. Cescon, Failure analysis of aluminum cable steel reinforced (ACSR) conductor of the transmission line crossing the Parana River, Eng. Fail. Anal. 9 (6) (2002) 645–664.
[3] A. Baltazar, C.D. Hernandez-Salazar, B. Manzanares-Martinez, Study of wave propagation in a multiwire cable to determine structural damage, NDT & E Int. 43 (8) (2010) 726–732.
[4] S.L. Branham, M.S. Wilson, S. Hurlebaus, B.M. Beadle, L. Gaul, Nondestructive testing of overhead transmission lines, in: Conference on Damage in Composite Materials, Stuttgart, 2006.
[5] G. Chen, X. Wang, J. Wang, J. Liu, T. Zhang, W. Tang, Damage investigation of the aged aluminium cable steel reinforced (ACSR) conductors in a high-voltage transmission line, Eng. Fail. Anal. 19 (2012) 13–21.
[6] COMSOL Inc., COMSOL Multiphysics®. <http://www.comsol.com/> (accessed September 2014).
[7] L. De Marchi, A. Marzani, M. Miniaci, A. Perelli, N. Testoni, Localization of defects in irregular waveguides by dispersion compensation and pulse compression, Proc. SPIE 8695 (2013) 869517–869527.
[8] Electric Power Research Institute, Investigation of Applying New Technologies to Overhead Transmission Line Inspections, Project 14972, September 1981.
[9] B. Engineer, The Mechanical and Resonant Behaviour of a Dry Coupled Thickness-shear PZT Transducer used for Guided Wave Testing in Pipe Line, Ph.D. Thesis, School of Engineering and Design, Brunel University, London, 2013.
[10] L. Gaul, H. Sprenger, C. Schaal, S. Bischoff, Structural health monitoring of cylindrical structures using guided ultrasonic waves, Acta Mech. 223 (8) (2012) 1669–1680.
[11] S.W. Golomb, Shift Register Sequences, Aegean Park Press, Laguna Hills, CA, 1982.
[12] T. Haag, B.M. Beadle, H. Sprenger, L. Gaul, Wave-based defect detection and interwire friction modeling for overhead transmission lines, Arch. Appl. Mech. 79 (6–7) (2009) 517–528.
[13] J.S. Hall, J.E. Michaels, D.O. Thompson, D.E. Chimenti, Adaptive dispersion compensation for guided wave imaging, in: AIP Conference Proceedings-American Institute of Physics, vol. 1430, 2012, pp. 623.
[14] Imperial College London, Disperse®. <http://www3.imperial.ac.uk/nde/products> (accessed September 2014).
[15] H.A. International, U.S. Helicopter Summary Statistics, 1996–2004.
[16] J. Katrasnik, F. Pernus, B. Likar, A survey of mobile robots for distribution power line inspection, IEEE Trans. Power Deliv. 25 (1) (2010) 485–493.
[17] P. Mudge, Field application of the Teletest long range ultrasonic testing technique, Insight 43 (2) (2001).
[18] Plant Integrity, Teletest®. <http://www.teletestfocus.com/teletest-focus-plus/> (accessed September 2014).
[19] M. Ricci, L. Senni, P. Burrascano, Virtual Instrument for Air-coupled Ultrasound NDT Application Based on Psuedo-noise Sequences, Relation 1000, 1, 2011.
[20] R. Sicard, J. Goyette, D. Zellouf, A numerical dispersion compensation technique for time recompression of Lamb wave signals, Ultrasonics 40 (1–8) (2002) 727–732.
[21] D. Siegert, P. Brevet, Fatigue of stay cables inside end fittings: high frequencies of wind induced vibrations, Bull.-Int. Organ. Study Endurance Ropes 89 (2005) 43.
[22] J. Snell, J. Renowden, Improving results of thermographic inspections of electrical transmission and distribution lines, in: ESMO 2000 Conference, 2000, pp. 135–144.
[23] T. Wiens, Kasami Sequences, m-sequences, Linear Feedback Shift Registers, 2009. <http://www.mathworks.com/matlabcentral/fileexchange/22716-kasami-sequences–m-sequences–linear-feedback-shift-registers/content/coding102/kasami.m> (accessed September 2014).
[24] P. Wilcox, A rapid signal processing technique to remove the effect of dispersion from guided wave signals, IEEE Trans Ultrason. Ferroelectr. Freq. Control 50 (4) (2003) 419–427.
[25] P. Wilcox, M. Lowe, P. Cawley, The effect of dispersion on long-range inspection using ultrasonic guided waves, NDT & E Int. 34 (1) (2001) 1–9.
[26] J. Xingliang et al., An s-transform and support vector machine (SVM)-based online method for diagnosing broken strands in transmission lines, Energies 4 (9) (2011) 1278–1300.
[27] K. Xu et al., Wideband dispersion reversal of Lamb waves, IEEE Trans Ultrason. Ferroelectr. Freq. Control 61 (6) (2014) 997–1005.

Please cite this article in press as: M. Legg et al., Increased range of ultrasonic guided wave testing of overhead transmission line cables using dispersion compensation, Ultrasonics (2015), http://dx.doi.org/10.1016/j.ultras.2015.04.009

[28] T. Yamasaki, S. Tamai, M. Hirao, Optimum excitation signal for long-range inspection of steel wires by longitudinal waves, NDT & E Int. 34 (3) (2001) 207–212.
[29] M.K. Yucel, M. Legg, M. Livadas, V. Kappatos, C. Selcuk, T.-H. Gan, Identification and Utilisation of Ultrasonic Guided Waves for Inspection of ACSR Cables, ECNDT 2014, October 2014.
[30] L. Zeng, J. Lin, Chirp-based pre-compensation for high resolution Lamb wave inspection, NDT & E Int. 61 (2014) 35–44.
[31] X. Zhang, Guangmin Sun, H. Liu, Q. Wang, Flaw classification in ultrasonic guided waves signal using wavelet transform and PNN classifier, in: 2011 International Conference on Wireless Communications and Signal Processing (WCSP), IEEE, Nanjing, 9–11 November 2011.

Please cite this article in press as: M. Legg et al., Increased range of ultrasonic guided wave testing of overhead transmission line cables using dispersion compensation, Ultrasonics (2015), http://dx.doi.org/10.1016/j.ultras.2015.04.009